

GOESR3 Periodic Reporting

Reporting Period: July 2018 – December 2018 (1st half of FY18 funding cycle)

Team Lead: Xuguang Wang (PI, OU)

Team Members: co-PIs Aaron Johnson (OU), Thomas Jones (OU), Jason Otkin (WI), Yanqiu Zhu (EMC)

Project Title: Assimilation of high resolution GOES-R ABI infrared water vapor and cloud sensitive radiances using the GSI-based hybrid ensemble-variational data assimilation system to improve convection initiation forecast.

Project Number: NA16OAR4320115

Executive Summary

The primary objectives of the project include (a) further extend the GSI EnKF/EnVar DA system for assimilating high resolution GOES-R ABI infrared water vapor and cloud sensitive radiance observations by ingesting convection resolving model's own high-resolution EnKF ensemble rather than the GFS ensemble and by directly updating cloud hydrometeor variables; (b) improve the usage of GOES-R ABI water vapor and cloud sensitive radiances for rapidly updated DA by refining data quality control, using high-resolution infrared land surface emissivity databases and exploring all-sky bias correction and observation error methods, and (c) test different DA configurations and evaluate the impact of assimilating GOES-R water vapor and cloud sensitive radiance observations for the prediction of diverse CI events when combined with ground based observation networks.

During this reporting period, further investigation of non-linear bias correction with different predictors has been conducted and the non-linear bias correction procedure has been implemented into the GSI-based EnKF. Experiments comparing the impact on a high-impact CI event of assimilating only radar observations vs. assimilating both radar and ABI channel 9 all sky radiance observations, using the existing multi-variable regression bias corrections were conducted. This experiment reveals the positive impact of assimilating ABI all sky radiance observations and provides a baseline for quantifying the impacts of our ongoing developments of bias correction and observation error specification for direct assimilation of all-sky IR radiances for CI prediction.

Progress toward FY17 Milestones

The project progresses as planned in general. Specifically, progress in the first half of FY18 has been focused on (A) further exploration of bias correction methods and (B) demonstrating the impact of assimilating all sky ABI radiances for the CI case using the current state of the art bias correction approach through data assimilation cycling experiment.

Specific progresses are summarized below.

A) EXPLORATION OF BIAS CORRECTION METHODS

In the last report, we showed that the non-linear bias correction method can effectively remove conditional biases from all-sky infrared brightness temperature when the observed brightness temperature is used as the bias predictor. During this reporting period, we explored different bias predictors using the same non-linear method, including observed cloud top height, total-column water content, satellite zenith angle, simulated brightness temperature, simulated cloud top height, and symmetric brightness temperature (e.g., average of the observed and simulated brightness temperatures). The effect of the non-linear correction terms is examined using all-sky brightness temperatures from ABI bands 8-10, that is, the upper-, mid-, and lower-level tropospheric water vapor bands.

Figures 1 and 2 depict the results for the upper-level water vapor band when using a subset of these bias predictors. Each figure shows 2-D probability distributions of the observation-minus-background (OMB) departures from the prior analyses plotted as a function of the predictor value along the x-axis. The horizontal red line is the mean bias of the entire distribution, whereas the short black lines depict the conditional bias in each column of the distribution. The top row shows the original distribution, the second row shows the OMB departure distributions after applying the 0th and 1st order (linear terms), and the bottom row shows the distributions after applying the linear and nonlinear (2nd and 3rd order) terms.

Overall, it is found that the non-linear bias correction terms were best able to remove biases from the all-sky OMB departures when the observed cloud top height or observed brightness temperature was used as the bias predictor. For those predictors, the nonlinear terms were able to effectively remove the conditional biases across the entire distribution for each of the water vapor bands, and meanwhile significantly reduced the variance in the entire OMB departures (Table 1). The non-linear terms also worked well when using the simulated brightness temperature, total water content at 100-700 hPa layer or simulated cloud top height as the bias predictor, as they were likewise able to remove the conditional biases for each of the water vapor bands but reduced the OMB departures to a lesser extent. The non-linear correction terms did not have much impact when using the satellite zenith angle or symmetric brightness temperature as the predictor because the OMB departures showed rather small systematic dependence on these predictors after linear bias correction, similar to that found in Otkin et al. (2018). Likewise, the nonlinear terms did not work when using symmetric cloud top height as the predictor.

During this report period, the aforementioned nonlinear bias correction is implemented in GSI. The GSI observer uses CRTM as the forward radiative transfer model to simulate the upwelling brightness temperature corresponding to GOES-R ABI channels. The first-guess profiles of temperature, humidity and hydrometeors are used as input to the CRTM. In the bias implementation, the observed brightness temperature is used as the predictor. Fig. 3 shows an example of the implementation using the ensemble mean first-guess model fields corresponding to the CI case on 1710 UTC of 18 May 2017. It can be seen that the first guess departure from the observation shows a large value especially with cold brightness temperature below 230 K. This is likely due to the high clouds present in those regions which can be confirmed from the cloud top pressure values derived from GOES-R radiances. It can also be seen that, the first guess departure from the observations is reduced after the nonlinear bias correction. The improvement is more evident, in the regions of cold observed brightness temperature.

B) IMPACT OF ASSIMILATING ALL SKY ABI RADIANCES

The 18 May 2017 case study of the convective initiation (CI) of rapidly evolving tornadic supercells, introduced in previous progress reports, is used to provide a baseline measure of the impact of assimilating ABI channel 9 all sky radiances. The data assimilation configuration consists of a 40-member ensemble at 3 km grid spacing with fixed physics (notably, the Thompson microphysics scheme), 17 cycles of hourly

assimilation of conventional surface and upper air observations from 0000 UTC through 1700 UTC, and 9 cycles of convective scale assimilation at 10 minute intervals from 1710 UTC through 1830 UTC. One experiment assimilates only the currently available NEXRAD radar observations during the latter period, while another experiment assimilates both the radar observations and the ABI channel 9 radiances. Deterministic forecasts are initialized from the ensemble mean analysis of each experiment at 1800, 1810, 1820 and 1830 UTC to understand how the advantage of assimilating the ABI observations changes as the event unfolds.

The main differences between the analyses with and without ABI radiance assimilation can be seen in the ensemble mean analysis brightness temperatures at 1800 UTC (Fig. 4). The first panel of Figure 4, showing the ABI channel 9 observed brightness temperatures over the region of interest, shows localized minima corresponding to towering cumulus clouds. These clouds are the first indication of impending CI and are observed by ABI radiance before the radar reflectivity (not shown). The radar-only assimilation experiment (center panel) has not yet picked up on these developing clouds at this time, as they are absent from the southern part of the center panel of Figure 4. Furthermore, there is remnant cloud in the northern part of the plotted region in the radar-only experiment where some spurious convection was removed from the model by the assimilation of clear air reflectivity. The experiment assimilating both radar and ABI observations (right panel of Figure 4) shows clear advantages over radar-only in both aspects. First, the developing clouds in the southern part of the plotted region are well analysed. Second, the suppression of spurious convection that was accomplished more quickly than with radar-only (not shown) is able to also include removal of the corresponding spurious cloud over the northern part of the plotted region (right panel of Figure 4).

The improved analyses are also carried over into improved forecasts resulting from assimilating the ABI radiance data (Fig. 5). When only assimilating radar data (top row of Figure 5), the 1900 UTC forecast does not pick up on the initiation of intense convection until the 1830 UTC initialization cycle (last column of top row of Fig. 5). In contrast, the experiment that also assimilates ABI channel 9 radiance data is able to better reproduce the forecast CI in the 1830 initialization (last column of bottom row of Fig. 5), and is even able to pick up on the CI event 10 minutes earlier in the 1820 initialization (second to last column of bottom row of Fig. 5). These experiments provide a quantitative baseline that is expected to be further improved upon through our further developments of e.g., the bias correction and observation error specification methods, as well as including surface sensitive IR channels.

Plans for Next Reporting Period

During the next reporting period, the exploration of non-linear bias correction will be extended to combine the predictors to minimize the O-B errors for the three bands and potentially other bands collectively, given the utility of different predictors varies with ABI bands. This will also lead to more rigorous tests of the impacts of different bias correction techniques on the CI forecast using the above experiments as a baseline for comparison. In addition, we plan to begin exploring methods to improve the estimate of the ABI radiance observation errors and studying the impact of different microphysics schemes on the ABI cloudy radiance assimilation.

1. Interaction with operational partners –

The proposing team interacted with NCEP/EMC collaborator Yanqiu Zhu during the extension and testing of the GSI EnKF system with the ABI clear air and cloudy radiance assimilation including pre-processing, QC, code modifications. The proposing team also interacts with NCEP/EMC collaborator Ming Chen on the implementation of high resolution surface emissivity with CRTM-CSEM.

2. Conference/workshop participation –

We continue participating the bi-weekly GSI developers meeting hosted by NCEP/EMC. We also presented our scientific results during the AMS annual meeting in Phoenix, AZ.

Johnson, A., X. Wang, T. A. Jones and J. Otkin, 2019: Improving Convection Initiation Forecasts by Assimilating High-Resolution *GOES-16* ABI Infrared Water Vapor and Cloud Sensitive Radiances Using GSI-Based EnKF/EnVar. AMS annual meeting, Phoenix.

3. Outside project publicity –

N/A during this project period.

4. Journal articles –

N/A during this project period as the primary effort is system development. Papers including scientific results will be submitted in the future.

Key Graphics

	Orig Var	Obs Tb	Obs Cld	TWC	SZA	Sim Tb	Sim Cld	Sym Tb
Band 8	24.45	-2.18	-4.19	-1.32	-0.22	-2.00	-1.06	-0.09
Band 9	45.35	-3.77	-8.12	-2.28	-0.54	-2.81	-0.16	-0.18
Band 10	72.37	-5.05	-12.47	-2.63	-0.90	-3.16	-0.33	-0.47

Table 1. Impact of the non-linear correction terms on the OMB departure distribution for ABI bands 8-10, as measured by changes in variance. Variance in original distribution is shown in column 2. Reductions in variance are shown in column 3 to 9 for experiments in which observed brightness temperature (Obs Tb), observed cloud top height (Obs Cld), total water content at 100-700 hPa layer (TWC), satellite zenith angle (SZA), simulated brightness temperature (Sim Tb), simulated cloud top height (Sim Cld), symmetric brightness temperature (Sym Tb), or symmetric cloud top height (Sym Cld) are used as the predictors, in order.

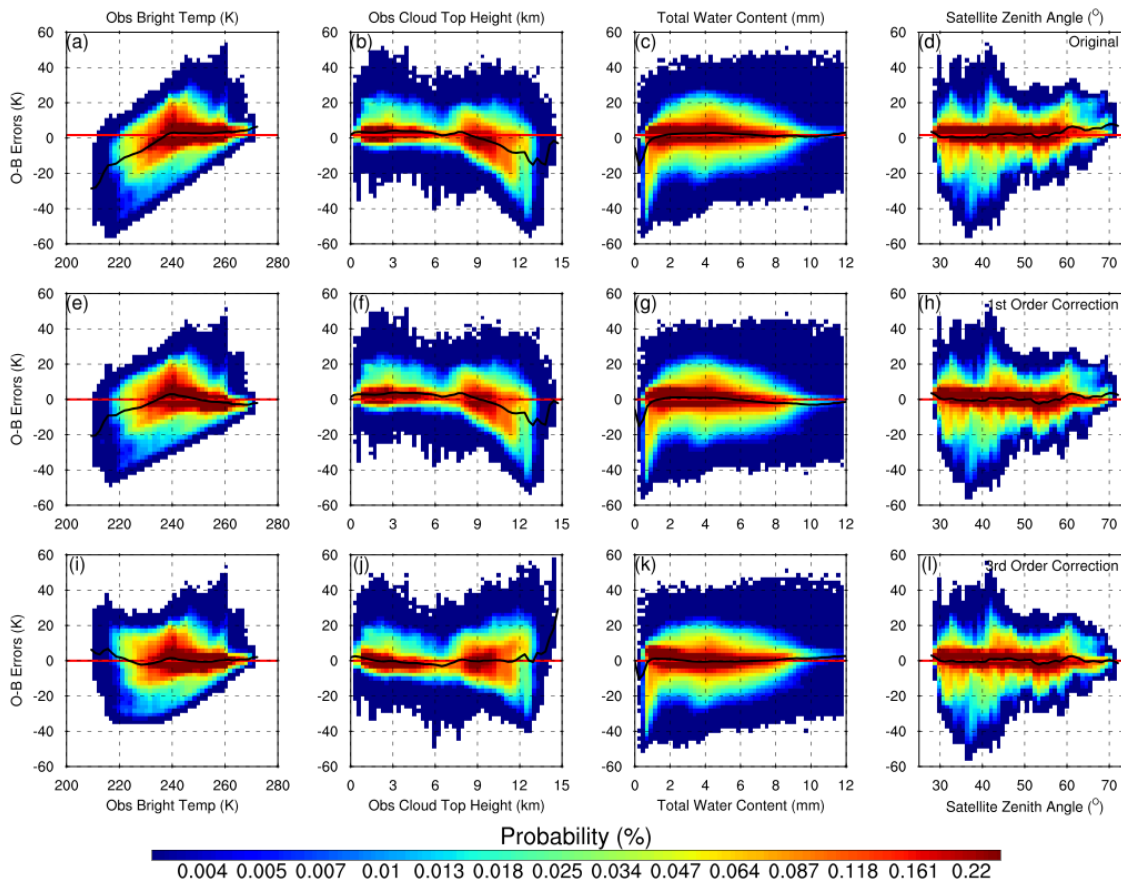


Figure 1. Probability distributions of 6.9 micron observation-minus-background departures plotted as a function of the observed 6.9 micron brightness temperatures for the (a) original data, and (e) 1st order and (i) 3rd order bias corrections when the observed 6.9 micron brightness temperatures are used as the bias predictor. (b, f, j) Same as above except when the observed cloud top height is used as the bias predictor. (c, g, k) Same as above except when the total water content is used as the bias predictor. (d, h, l) Same as above except when the satellite zenith angle is used as the bias predictor. The horizontal black line segments in each panel represent the conditional bias in each column, whereas the red line shows the mean bias of the entire distribution. The distributions were generated using data from 7 assimilation cycles in which the 6.9 micron brightness temperatures were passively monitored.

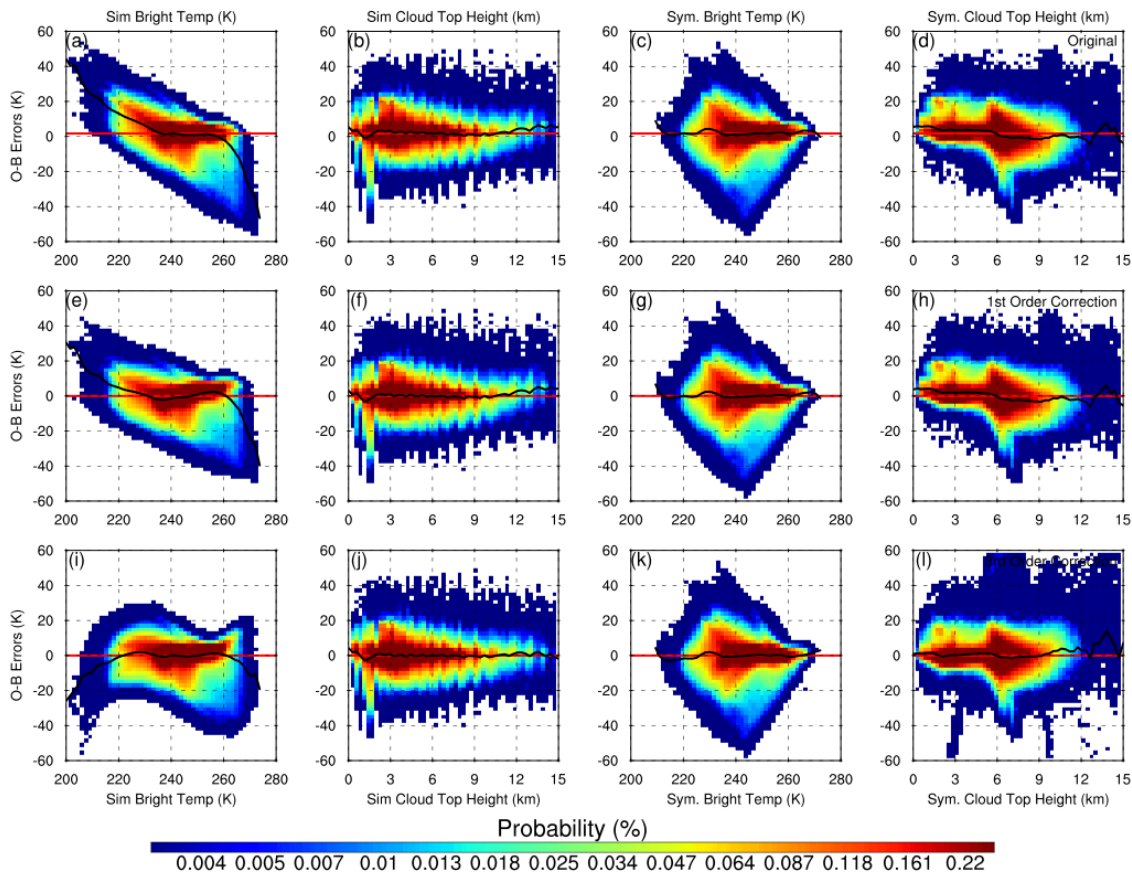


Figure 2. Probability distributions of 6.9 micron observation-minus-background departures plotted as a function of the simulated 6.9 micron brightness temperatures for the (a) original data, and (e) 1st order and (i) 3rd order bias corrections when the simulated 6.9 micron brightness temperatures are used as the bias predictor. (b, f, j) Same as above except when the simulated cloud top height is used as the bias predictor. (c, g, k) Same as above except when the symmetric brightness temperature is used as the bias predictor. (d, h, l) Same as above except when the symmetric cloud top height is used as the bias predictor. The horizontal black line segments in each panel represent the conditional bias in each column, whereas the red line shows the mean bias of the entire distribution. The distributions were generated using data from 7 assimilation cycles in which the 6.9 micron brightness temperatures were passively monitored.

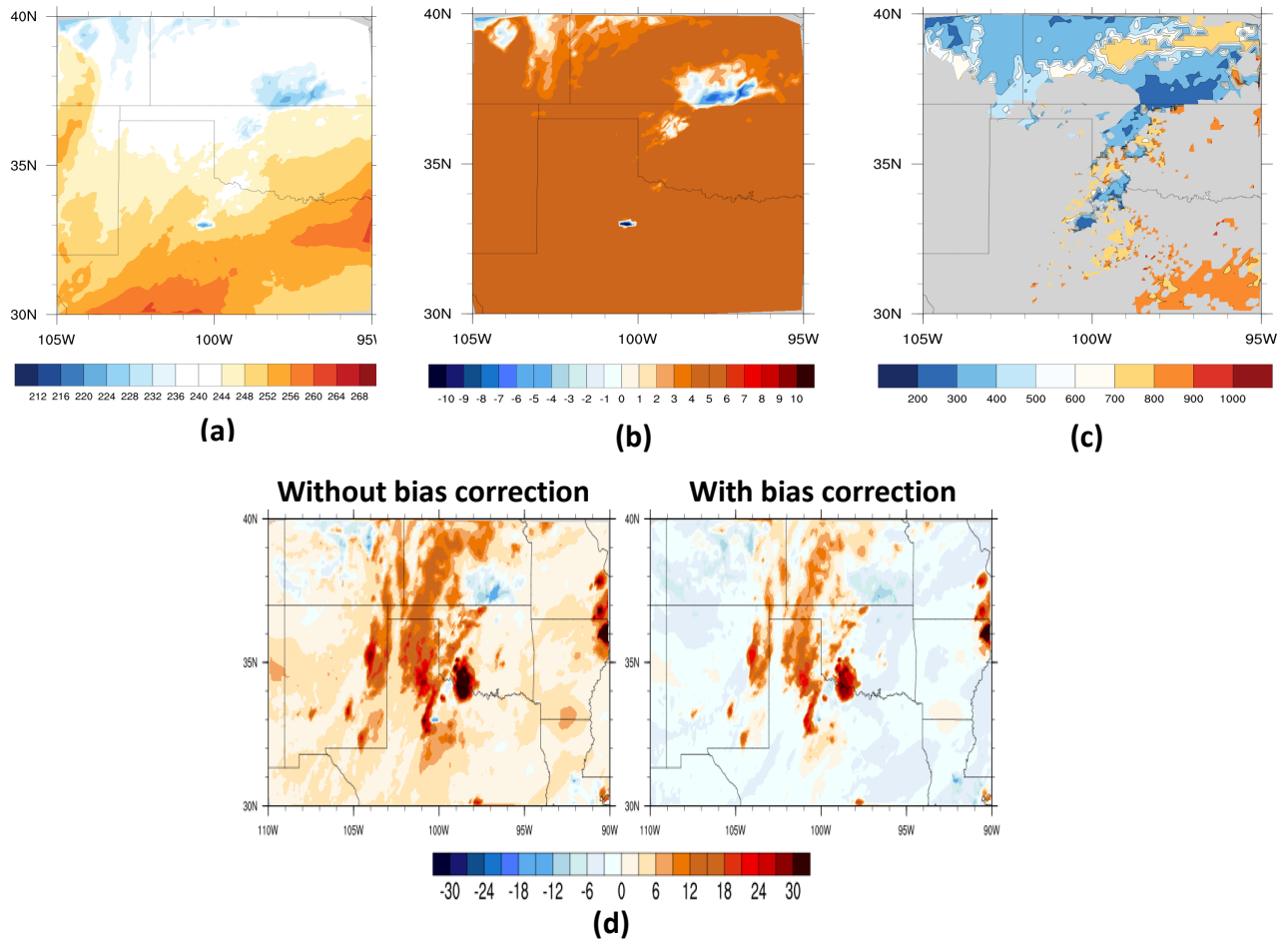


Figure 3. (a) Observed Channel 9 brightness temperature in K, (b) Total bias in K, predicted with Channel 9 observation as predictor using the non-linear bias correction technique for ensemble mean first guess at 1710 UTC of 18 May 2017, (c) cloud top pressure values derived from GOES-R observations and (d) Observation-minus-background departures in K, for 6.9 micron channel without / with bias correction .

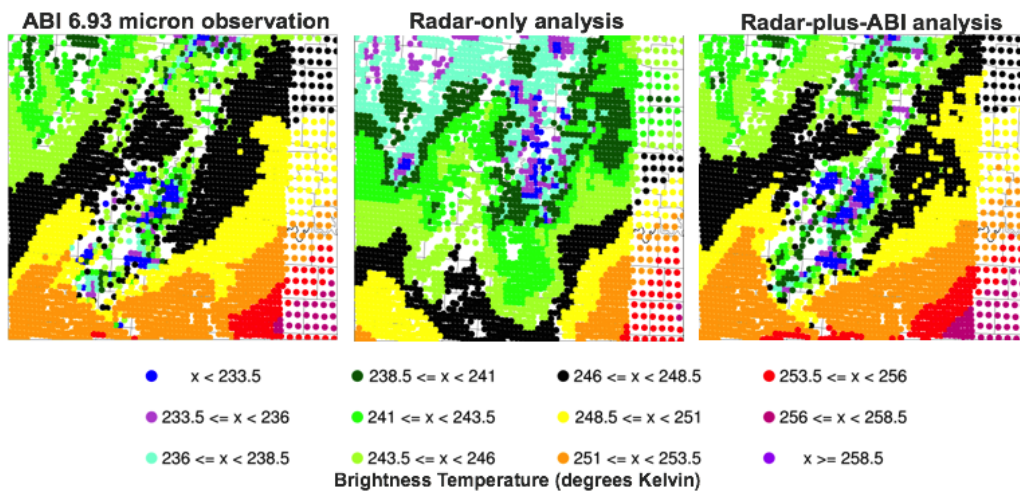


Figure 4. 6.93 micron brightness temperature at 1800 UTC 18 May 2018 in (left) observations, (center) radar-only experiment ensemble mean analysis and (right) radar-plus-ABI experiment ensemble mean analysis.

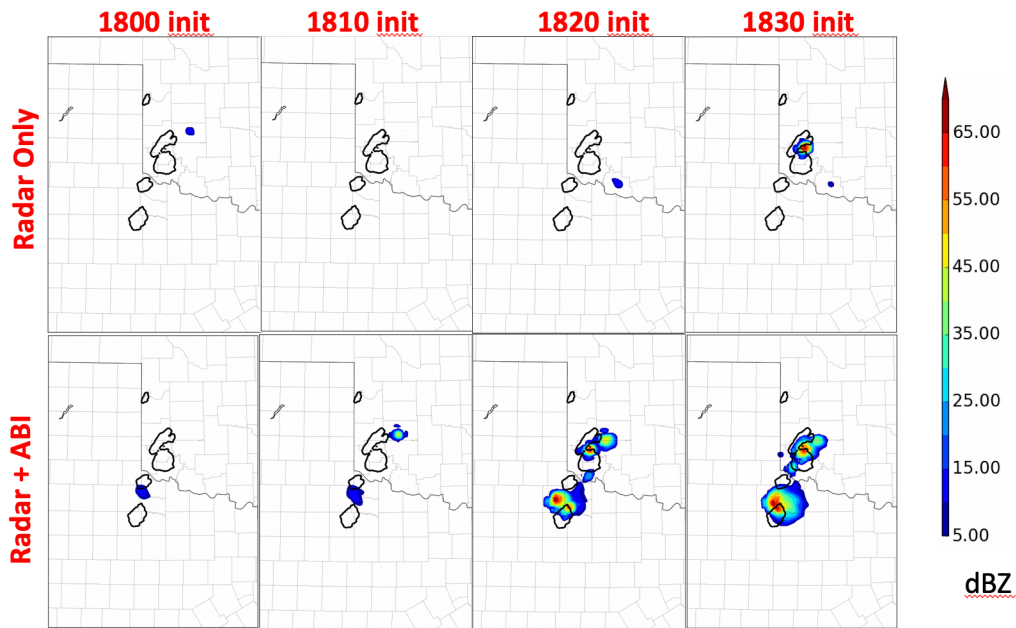


Figure 5. Forecasts of reflectivity (shaded) and observed 35 dBZ reflectivity (black contour) for forecasts initialized at different times (columns) from different experiments (rows). All forecasts are valid at 1900 UTC.